On the Fluid Mechanics of Spiral−Wound Membrane Modules

ARTICLE *in* INDUSTRIAL & ENGINEERING CHEMISTRY RESEARCH · NOVEMBER 2009

Impact Factor: 2.59 · DOI: 10.1021/ie901129j

2 AUTHORS:

Margaritis Kostoglou
Aristotle University of Thessaloniki
165 PUBLICATIONS **2,067** CITATIONS
SEE PROFILE

Anastasios J. Karabelas
The Centre for Research and Technology, …
288 PUBLICATIONS **4,420** CITATIONS
SEE PROFILE

On the Fluid Mechanics of Spiral-Wound Membrane Modules

M. Kostoglou[†] and A. J. Karabelas*[,‡]

Division of Chemical Technology, Department of Chemistry, Aristotle University, GR 541 24 Thessaloniki, Greece and Chemical Process Engineering Research Institute, Centre for Research and Technology, Hellas, sixth km Charilaou-Thermi Road, GR 570 01, Thermi-Thessaloniki, Greece

Spiral-wound membrane (SWM) modules are comprised of several large-size membrane sheets with a net-type spacer at the retentate flow channel and a porous cloth/filler at the low-pressure permeate side; thus, two strongly interacting flow fields exist with spatially variable properties. Mathematical models of the SWM operation, based on an accurate description of transport phenomena taking place in those narrow flow passages, are necessary tools for optimizing both module design parameters and the entire membrane-based plant. Such integrated SWM models are not available at present. In this problem, the coexistence of several flow length scales, from the pores of the permeate side filler to the macroscopic dimensions of the module, renders the modeling task quite complicated. Typical modeling efforts vary between the extremes of detailed description of transport phenomena at small scale to macroscopic phenomenological-type simulation of the entire separation process in a module. The scope of this work is to describe the hydrodynamics of spiral-wound membranes, starting from first principles, to suggest and analyze some realistic approximations and their origin and to present an integrated model where linking phenomena at different length scales is an essential feature. This effort has resulted in an efficient numerical algorithm, allowing predictions of the spatial distribution of pressure, permeation, and cross-flow velocities throughout the membrane leaves. In this work, all possible analytical solutions have been derived which facilitate the development of the simulation algorithm. Typical examples of predicted flow and pressure distributions are presented.

1. Introduction

During the past 20 years the membrane filtration operation was established as a competitive, and in many cases most attractive, option for a great variety of separation processes, in the broad field of water treatment[1] and elsewhere. Currently available membrane modules include spiral-wound, hollow-fiber, tubular, and plate and frame elements, employed in reverse osmosis, nanofiltration, ultrafiltration, and microfiltration operations. The hollow-fiber and spiral-wound modules are more common than the others, mainly due to their higher area to volume ratio. The spiral-wound modules (SWM) have distinct advantages[1] over the hollow-fiber elements, in important applications, although the latter can offer higher packing density. In general, SWM currently dominate the market of reverse osmosis (RO) and nanofiltration (NF) plants, with significant applications in ultrafiltration processes as well. The present work addresses, in general, the problem of hydrodynamics of spiral-wound modules, which is common to all the above filtration modes; however, in this paper special attention is paid to the high-pressure operations (RO, NF) which tend to be more complicated (at least from the modeling stand point) due to the filtration-induced phenomena of concentration polarization, although such phenomena manifest themselves in some low-pressure operations as well. Furthermore, the present study, although restricted to the fluid dynamics problem, aims at developing, in a systematic manner, a sound basis for extension to an integrated modeling tool by taking into account the mass transfer problem as well.

SWM modules are comprised of several large-size membrane sheets separated by a net-type spacer at the feed/retentate flow channel and a porous cloth/filler at the low-pressure permeate side; therefore, two strongly interacting flow fields exist on either side of each membrane with spatially variable properties. It is evident that the performance of the spiral-wound modules is affected by many factors, related mainly to flow geometry and fluid dynamics, thus necessitating optimization of both module design and operating parameters.[2] Appropriate mathematical models of SWM operation are, therefore, valuable tools for such optimization. It should be noted here that although the basic phenomena, occurring during the steady state and smooth operation (i.e., with no fouling) of RO/NF membranes, are relatively well understood, their quantitative description is difficult due to the geometrical complexity of the spiral-wound elements. Actually, transport phenomena in SWM take place over several length scales, from the pores of the permeate side filler to the macroscopic dimensions of the element, with the most important size scales being those associated with the spacers in the retentate channel.

Although several modeling attempts can be found in the older literature,[3−5] extensive use of the SW membranes in recent years has led to an increased interest in their simulation. A relatively recent review[2] provides a useful summary of relevant simulation efforts. In general, the following categorization of the modeling efforts may be made: first, some works are focused only on the fluid dynamics, while others deal with the simulation of the complete separation process, albeit in a simplified manner. Another distinction may be made between studies attempting a geometrically detailed flow description for the retentate side and those employing mesoscopic volume-averaged equations. The detailed flow description for the entire length of the membrane element is practically possible at present only for a simplified 2-dimensional geometry, and even then it requires a substantial computational effort.[6] The most common and fruitful approach for a detailed flow description is that of a periodic unit cell[7−9] in which the simulation is restricted to a small part of the module, thus permitting the realization of 3-dimensional

* To whom correspondence should be addressed. E-mail: karabaj@cperi.certh.gr.
[†] Aristotle University of Thessaloniki.
[‡] Chemical Process Engineering Research Institute-CERTH.

10.1021/ie901129j CCC: $40.75
Published on Web 10/23/2009

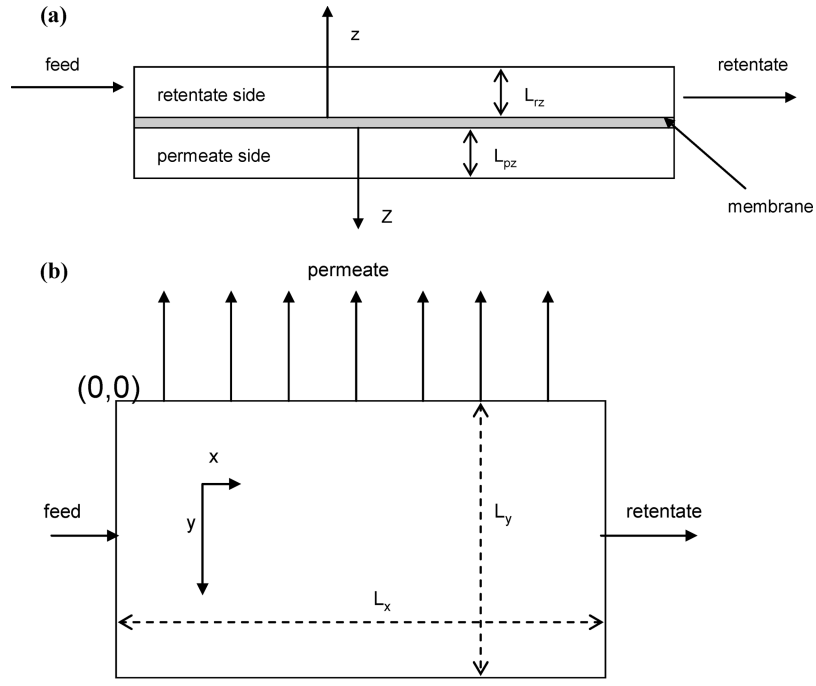

Figure 1. Schematic of the simplified membrane element geometry considered: (a) cross-sectional view and (b) top view of membrane sheet.

simulations.[10−13] Commercial computational fluid dynamics (CFD) codes are commonly used for this type of modeling. On the other hand, the mesoscopic models are solved either using in-house codes based on numerical techniques for handling differential equations (Runge−Kutta,[14] finite differences employing Crank−Nickolson,[4] or Newton−Raphson techniques[15]) or by developing approximate analytical solutions.

A review of relevant studies suggests that essentially all the elements required for simulating flow in spiral-wound modules can be found in the literature, although they are quite dispersed among models of different scales and different degrees of approximation. The scope of this work is to present and analyze the hydrodynamics of the spiral-wound module (in the absence of solute), starting from first principles, and to explain in sufficient detail the necessary approximations made (and their origin) in linking the various flow field length scales. In this effort, all possible analytical solutions are derived and presented. The work results in an optimized numerical algorithm that accounts for the spatial variation of pressure and velocity in the membrane module. The presentation starts with a complete problem formulation and analysis for both the feed and permeate channels of the module; problem solution follows, as well as indicative results under conditions of practical interest.

2. Problem Formulation

The geometry of a membrane element is shown in Figure 1. The element is assumed to be a flat sheet instead of a wrapped one since the ratio of its thickness (and of the associated channel gaps) to the radius of curvature is small.[16] According to recent studies,[17,18] curvature has some influence, but this issue will not be considered here. The dimensions of the membrane sheet are L_x and L_y, whereas the gap of the permeate and retentate channel (considered in the flow calculations) is L_{pz} and L_{rz}, respectively. The coordinate system considered here is shown in Figure 1. This coordinate system may not be straightforward, but it leads to the simplest mathematical description of the problem. The two coordinates x, y are common for both permeate and retentate sides, but the third coordinate is different. Both coordinates z (for retentate side) and Z (for permeate side) have their origin on the corresponding membrane surface. It is noted that the following equations correspond to the case of a single membrane "unit" consisting of the membrane sheet and the two neighboring channels (i.e., for feed and permeate fluid). However, the results of the present study can be generalized for the case of a stack of parallel "units" comprising the module by appropriate modification of the mesoscopic mass balances.

2.1. Permeate Side Equations. The permeate channel is filled with a porous medium having pores much smaller than the channel thickness. In this case, for pore scale Reynolds number much smaller than 1, Darcy's law can be used, as discussed in Appendix A. For the sake of generality, the medium is assumed anisotropic with different permeabilities in directions parallel (k_1) and transverse (k_2) to the membrane, i.e.

$$u_p = -\frac{k_1}{\mu}\frac{\partial P}{\partial x} \tag{1a}$$

$$v_p = -\frac{k_1}{\mu}\frac{\partial P}{\partial y} \tag{1b}$$

$$w_p = -\frac{k_2}{\mu}\frac{\partial P}{\partial Z} \tag{1c}$$

where u_p, v_p, and w_p are the three components of the velocity and P is the pressure in the permeate channel. The liquid mass balance in the permeate channel is as follows ($\vec{U}_p$ is the vector notation for the velocity)

$$\vec{\nabla}\vec{U}_p = 0 \tag{2}$$

which, after substitution of eqs 1a, 1b, and 1c, results in

$$\frac{\partial^2 P}{\partial x^2} + \frac{\partial^2 P}{\partial y^2} + \frac{k_2}{k_1}\frac{\partial^2 P}{\partial Z^2} = 0 \tag{3}$$

in the domain defined by $0 < Z < L_{pz}$, $0 < x < L_x$, and $0 < y < L_y$.

The boundary conditions (i.e., no flux at the solid walls located at $x = 0$, $x = L_x$, $y = L_y$, $Z = L_{pz}$ and known pressure at the permeate outlet at $y = 0$) are

$$x = 0 \text{ and } x = L_x\text{: } \frac{\partial P}{\partial x} = 0 \tag{4a}$$

$$y = 0\text{: } P = P_{out} \tag{4b}$$

It is very convenient to define all pressures in the problem so that for outflow $P_{out} = 0$; this is permitted due to the structure of the problem

$$y = L_y\text{: } \frac{\partial P}{\partial y} = 0 \tag{4c}$$

$$Z = L_{pz}\text{: } \frac{\partial P}{\partial Z} = 0 \tag{4d}$$

2.2. Retentate (Feed) Side Equations. The inserts (spacers) in this channel are of size comparable to the channel thickness, so the full Navier−Stokes equations must be considered. The Reynolds number of practical interest is on the order of 100, which creates several complications to the flow such as an inherent unsteadiness.[7] It will be stressed that in practice the Reynolds number in the two flow compartments usually differs by more than 2 orders of magnitude due to the fact that the mean flow in the permeate channel is only a small fraction (i.e., less than 5%) of that in the retentate side; additionally, the size of the filler pores in the permeate channel is much smaller than the length scale of the feed side spacers. In the domain $0 < z < L_{rz}$, $0 < x < L_x$, and $0 < y < L_y$, the following system describes the flow

$$\frac{\partial u_r}{\partial x} + \frac{\partial v_r}{\partial y} + \frac{\partial w_r}{\partial z} = 0 \tag{5a}$$

$$\frac{\partial u_r}{\partial t} + u_r\frac{\partial u_r}{\partial x} + v_r\frac{\partial u_r}{\partial y} + w_r\frac{\partial u_r}{\partial z} = -\frac{1}{\rho}\frac{\partial p}{\partial x} + \frac{\mu}{\rho}\left(\frac{\partial^2 u_r}{\partial x^2} + \frac{\partial^2 u_r}{\partial y^2} + \frac{\partial^2 u_r}{\partial z^2}\right) \tag{5b}$$

$$\frac{\partial v_r}{\partial t} + u_r\frac{\partial v_r}{\partial x} + v_r\frac{\partial v_r}{\partial y} + w_r\frac{\partial v_r}{\partial z} = -\frac{1}{\rho}\frac{\partial p}{\partial y} + \frac{\mu}{\rho}\left(\frac{\partial^2 v_r}{\partial x^2} + \frac{\partial^2 v_r}{\partial y^2} + \frac{\partial^2 v_r}{\partial z^2}\right) \tag{5c}$$

$$\frac{\partial w_r}{\partial t} + u_r\frac{\partial w_r}{\partial x} + v_r\frac{\partial w_r}{\partial y} + w_r\frac{\partial w_r}{\partial z} = -\frac{1}{\rho}\frac{\partial p}{\partial z} + \frac{\mu}{\rho}\left(\frac{\partial^2 w_r}{\partial x^2} + \frac{\partial^2 w_r}{\partial y^2} + \frac{\partial^2 w_r}{\partial z^2}\right) \tag{5d}$$

where u_r, v_r, and w_r are the three components of the velocity and p is the pressure in the retentate side channel.

It should be also noted that there is a connected space $V(x,y,z)$, with the corresponding surface $A_s(x,y,z)$, describing the solid inserts/spacers.

2.2.1. Boundary Conditions. Zero velocity on the side walls

$$\text{at } z = L_{rz},\ u_r = v_r = w_r = 0 \tag{6a}$$

$$\text{at } y = 0,\ y = L_{py},\ u_r = v_r = w_r = 0 \tag{6b}$$

No slip on the membrane surface

$$\text{at } z = 0,\ u_r = v_r = 0 \tag{6c}$$

Pressure definition at the inlet and outlet of the retentate channel

$$x = 0,\ p = p_{in} \tag{6d}$$

$$x = L_x,\ p = p_{out} \tag{6e}$$

Zero velocity on spacers

$$\text{at } A_s(x,y,z),\ u_r = v_r = w_r = 0 \tag{6f}$$

It is noted that, at first glance, a boundary condition on the inlet velocity (i.e., feed flow rate, which is the primary parameter of the problem) seems to be more reasonable; however, it is not so as it introduces an artificial behavior to the 3-dimensional problem. Indeed, a uniform inlet velocity profile is not appropriate because the true profile will adjust itself according to the local flow resistance. Thus, the correct procedure is to impose pressure boundary conditions and calculate the flow rate as the result.

2.2.2. Coupling the Two Flow Compartments Separated by the Membrane. The two compartments are obviously coupled through the permeation velocity U_w as follows

$$U_w = \frac{k_w}{\mu\delta}(p - P) \tag{7}$$

$$\text{retentate side: at } z = 0,\ w_r = -U_w \tag{8a}$$

$$\text{permeate side: at } Z = 0,\ \frac{\partial P}{\partial Z} = -\frac{\mu}{k_2}U_w \tag{8b}$$

Here, k_w is the permeability and δ the thickness of the membrane layer.

To understand the nature of the solid structure, at the retentate side, described by the function $V(x,y,z)$, the so-called spacers, one can inspect Figure 2. Evident is the periodic structure of the spacer geometry comprised of two (nonwoven) arrays of parallel cylindrical filaments, "intersecting" at an angle β, with the main flow symmetrically arranged at an angle $\theta = 90°$. In principle, other arrangements of the spacer with respect to the mean flow are possible (with angles θ other than 90°), but it has been shown that the symmetric arrangement is preferable.[10] Also, spacers made of filaments of noncircular cross section (rectangular, triangular) have been studied and found to be inferior to those of circular cross section.[19] The unit cell of the periodic structure shown in Figure 2 is characterized by the angle β (being a key structural parameter) and the ratio H/D of filament distance H over its diameter D. Determination of optimum spacer geometrical parameters (H/D and β) is a difficult task that is still under investigation. Such an optimum apparently depends[10,11] on the particular SWM application (e.g., high-pressure RO versus low-pressure UF, good vs poor quality of feed), although there are suggestions that in general the optimum value of β is a function of the flow conditions.[20]

The mathematical problem for the retentate side is now complete and well posed, but its numerical solution seems

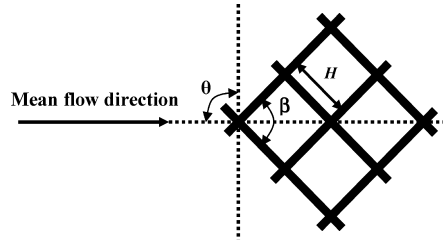

Figure 2. Top view of a spacer. A square-type ($\beta = 90°$) unit cell is shown comprised of two layers of parallel, nonwoven cylindrical filaments of diameter D; H is the distance between center lines of neighboring parallel filaments.

intractable due to two types of complexities. First, there is geometric complexity, i.e., to adequately capture the geometric details (especially in the regions of contact between solid surfaces−membrane/spacers) a huge number of discretization elements is required.[7,10] The computational cost for direct numerical simulation of the entire membrane element, comprised of thousands of unit cells, appears to be prohibitive at present. The second complexity originates from the relatively high Reynolds number of the retentate flow in the membrane element. The flow is inertia dominated, and it is inherently unsteady, exhibiting fine flow structures that need high spatial and temporal resolution to be described.[7,10] A way to proceed is to explore the periodic structure of the geometry, although the introduction of some assumptions and approximations is unavoidable, as will be subsequently discussed. The key point here is that the unit cell length scale (on order of a few millimeters) is very small compared to the macroscopic characteristic length of the flow (in this case the element dimensions, on order 10^2 cm). This permits, in principle, decomposition of the flow into two scales, i.e., the local unit cell fine scale and the macroscopic scale which can be solved simultaneously by proper communication of variables between them.

In the case of sufficiently small Reynolds numbers the flow is steady and the problem is linear, so that a strict mathematical procedure, well known as the method of multiple scales, can be employed. The method is actually a perturbation expansion having as perturbation parameter the ratio of the unit cell size to macroscopic size. A description of the method in the general context of perturbation methods is given by Kevorkian and Cole,[21] and its very detailed application to the particular field of transport in periodic structures can be found in the book by Brenner and Edwards.[22]

For the macroscopic flow (in the limit of small Reynolds number), the particular mathematical technique results in an equation similar to the empirical Darcy law

$$\vec{U} = \frac{1}{\mu}\underline{\mathrm{K}}\vec{G} \tag{9}$$

It is noted that the macroscopic flow field is a two-dimensional one since the z dimension is totally "absorbed" in the unit cell scale. Indeed, the velocity $\vec{U}$ is considered to depend only on x and y as it is the local velocity averaged over z. The symbol $\vec{G}$ represents the pressure gradient, and $\underline{\mathrm{K}}$ is the so-called permeability tensor, which depends only on the geometry of the unit cell. In case the structure of the unit cell implies invariance under some set of rotations/reflections, a priori available information about the form of the permeability tensor can be considered. In the present case the form of the unit cell allows the reduction of the independent scalar components of the permeability tensor from 4 to 2, i.e., $\underline{\mathrm{K}} = k_1\vec{i}\vec{i} + k_2\vec{j}\vec{j}$. The scalar permeabilities can be obtained by solving the unit cell problem imposing a mean pressure gradient in the x and y directions, respectively. In the particular case of a rectangular unit cell ($\beta = \pi/2$), the medium is isotropic ($k_1 = k_2$) and only one unit cell problem must be solved. For any other value of β, the medium is anisotropic ($k_1 \neq k_2$).

In the case of a finite Reynolds number, small enough to ensure a steady local flow field, the corresponding mathematical formulation exists[23] (as discussed in Appendix B), but its practical value is really restricted. The usual approach of accounting for the inertia for structured or unstructured porous media is through empirical laws like the Ergun equation[24] or through the use of the Forcheimer coefficient.[25] However, for higher Re number the unit cell flow field is not at steady state and there may be interaction between flow oscillations taking place in neighboring cells, possibly leading to a truly nonperiodic flow field. Although this has not been shown for the real spacer geometry, there is some evidence in the 2-dimensional approximation studied,[7] where a unit cell of two spacers gives somewhat different results than the unit cell of one spacer. The significance of possible deviation from flow periodicity cannot be rigorously assessed at present, although mass transfer measurements[12] indicate that it may not be important. Nevertheless, a convenient way to proceed (as discussed in Appendix B) is to adopt the multiple scales method not in its rigorous form but as a semiempirical approach. In the case of an unsteady unit cell flow field, time averaging is also required to extract parameters from the unit cell problem.

An additional complication stems from the fact that the nonlinearity of the governing equations invalidates any simplification emerging from the symmetry. In the nonlinear case (finite Reynolds number) not only the permeability tensor components are all nonzero but they are also functions of the magnitude and direction (e.g., angle θ) of the local velocity vectors. This means that the two values k_1,k_2 needed for the zero Reynolds number case are replaced by $k_{11}(\theta, U)$, $k_{22}(\theta,U)$ and $k_{12}(\theta,U) = k_{21}(\theta,U)$. The corresponding simulations needed to extract the unit cell parameters are increased from 2 to more than 100; indeed, assuming that at least 10 values of each variable (U,θ) are needed to determine the dependence of f_1,f_2 on U,θ, a total of $10 \times 10 = 100$ simulations are required. At this time all this information is not available. On the other hand, the function $k_{11}(\pi/2,U)$ can be obtained from simulations presented in the literature for several structures of the spacer matrix. In order to proceed using the existing information, one can invoke the fact that under practical conditions the direction of the "local" macroscopic velocity does not deviate much from the mean flow direction, which will be subsequently confirmed in this work. This leads to the assumption that the results obtained for $\theta = \pi/2$ can be also used for slightly different values of θ. In addition, it is assumed that the flow maintains the same direction with the pressure drop even if θ is not $\pi/2$. The above assumptions mathematically are expressed as $k_{11}(\theta,U) = k_{22}(\theta,U) = k_{11}(\pi/2,U)$ and $k_{12}(\theta,U) = k_{21}(\theta,U) = 0$.

Extensive unit cell flow field simulation results (using a commercial CFD code), over a rather broad parameter space,[10] show that the pressure drop along the flow direction for $\theta = \pi/2$ is given by an expression of the form

$$\frac{\Delta p}{\Delta L} = -f_1 \mathrm{Re}^{-f_2}\frac{U^2\rho}{D} \tag{10}$$

where the Reynolds number is defined as $\mathrm{Re} = UD\mu/\rho$ and ρ and μ are the fluid density and viscosity, respectively. The unit cell flow field simulations ignore the permeate, assuming that the flow through the membrane does not influence the retentate flow resistance. This assumption is justified[10] on the basis that the flux through the membrane in a unit cell (and throughout a membrane leaf) is on the order of 1/1000 of the retentate flow velocity; thus, the error, by neglecting it, is expected to be quite small and likely smaller than the errors introduced by other assumptions (e.g., periodicity). The coefficients f_1 and f_2 depend on spacer geometric parameters (H/D and β), and in general, they can be obtained from CFD simulations[10] by employing the unit cell approach. In the case of flow in an empty channel (no spacers), the pressure drop is dominated by the wall friction losses and $f_2 = 1$. In the case of flow past bluff bodies, the exponent f_2 is unity at very small Reynolds number and tends to 0 as the Reynolds number increases and the influence of

inertia on the pressure drop dominates. For narrow channels with spacers and for practical Reynolds numbers on the order of 10^2, f_2 is between 1 and 0 and according to the literature[10] closer to the inertia regime ($f_2 < 0.33$). Treating the macroscopic case and solving for the velocity, eq 10 is transformed to

$$U = -\frac{D^{1+f_2}}{f_1 U^{1-f_2}\rho^{1-f_2}\mu^{f_2}}\frac{\partial p}{\partial x} \tag{11}$$

Generalizing the above relation in the two-dimensional space, according to the analysis previously described, leads to

$$\vec{U} = -\frac{D^{1+f_2}}{f_1 U^{1-f_2}\rho^{1-f_2}\mu^{f_2}}\nabla p \tag{12}$$

and

$$U = \left(\frac{D^{1\ +\ f_2}}{f_1\rho^{1-f_2}\mu^{f_2}}|\nabla p|\right)^{1/(2-f_2)} \tag{13}$$

The local mass balance in the macroscopic scale, including the flow through the wall, leads to the following relation

$$L_{rz}\nabla\vec{U} = \frac{k_w}{\delta}(P-p) \tag{14}$$

where the mean local pressure p in this case is the time and z-direction average of the point pressure in the channel, which is a function of x and y.

Substitution of eqs 12 and 13 in the mass balance results in

$$\nabla|\nabla p|^{(f_2-1)/(2-f_2)}\nabla p = \left(\frac{f_1\rho^{1-f_2}\mu^{f_2}}{D^{1\ +\ f_2}}\right)^{1+(f_2-1)/(2-f_2)}\frac{k_w}{\delta L_{rz}}(p-P) \tag{15}$$

This is the final equation from which the 2-dimensional pressure distribution in the retentate channel can be computed.

2.3. Permeate Side Analytical Solution and Reformulation of the Problem. The linearity of the permeate side mathematical problem permits an analytical handling despite its three-dimensional nature. Assuming that $P = X(x)Y(y)W(Z)$, substituting in eq 3 and dividing by XYW results in

$$\frac{X''}{X} + \frac{Y''}{Y} + \frac{k_2}{k_1}\frac{W''}{W} = 0 \tag{16}$$

where the prime denotes differentiation of the function with respect to its argument. Obviously, each term in the above equation depends only on one independent variable, so it can be set equal to a constant. The x term is set equal to $-\lambda^2$ and the y term equal to $-\kappa^2$. In this way, three one-dimensional boundary value problems arise. The general solution of x and y problems is given in terms of trigonometric functions. Application of the corresponding boundary conditions (eq 4a for the x problem and eqs 4b and 4c for the y problem) leads to

$$X = \cos\left(\frac{i\pi}{L_x}x\right) \tag{17}$$

$$Y = \sin\left(\frac{j\pi}{2L_y}y\right) \tag{18}$$

The W equation is solved in terms of exponential functions, and after the application of boundary condition eq 4d one obtains

$$W = e^{-\beta_{ij}Z} + e^{\beta_{ij}(Z-2L_{pz})} \tag{19}$$

where

$$\beta_{ij} = \left(\frac{k_1}{k_2}\right)^{1/2}\left[\left(\frac{i\pi}{L_x}\right)^2 + \left(\frac{j\pi}{2L_y}\right)^2\right]^{1/2} \tag{20}$$

This solution can be also given in terms of hyperbolic sine and cosine functions, but simple exponentials are preferred here because their use is more straightforward. Using the principle of superposition, the general solution for the pressure field P is given as

$$P = \sum_{i=0}^{\infty}\sum_{j=1}^{\infty} a_{ij}(e^{-\beta_{ij}Z} + e^{\beta_{ij}(Z-2L_z)})\cos\left(\frac{i\pi}{L_x}x\right)\sin\left(\frac{j\pi}{2L_y}y\right) \tag{21}$$

where the coefficients a_{ij} must be determined from the boundary condition on the membrane. This condition takes the following form by combining eqs 7 and 8b

$$\frac{\partial P}{\partial Z} = \frac{k_w}{k_2\delta}(P-p) \ \text{ at } \ Z = 0 \tag{22}$$

The retentate pressure field $p(x,y)$ is expanded in terms of trigonometric functions as follows

$$p = \sum_{i=0}^{\infty}\sum_{j=1}^{\infty} e_{ij}\cos\left(\frac{i\pi}{L_x}x\right)\sin\left(\frac{j\pi}{2L_y}y\right) \tag{23}$$

where

$$e_{ij} = \frac{4}{L_x L_y}\int_0^{L_x}\int_0^{L_y} p(x,y)\cos\left(\frac{i\pi}{L_x}x\right)\sin\left(\frac{j\pi}{2L_y}y\right)\mathrm{d}x\,\mathrm{d}y \tag{24}$$

Substituting eqs 21 and 23 in the boundary condition eq 22, after some algebra, leads to

$$a_{ij} = \frac{e_{ij}}{\beta_{ij} - \beta_{ij}e^{-2\beta_{ij}L_{pz}} + \frac{k_w}{k_2\delta}(1 + e^{-2\beta_{ij}L_{pz}})} \tag{25}$$

Therefore, an analytical solution (eqs 21, 24, and 25) for the three-dimensional permeate pressure field $P(x,y,z)$ in terms of the retentate flow field $p(x,y)$ was derived.

It is worth noting that, using this analytical solution, the retentate side problem can be separated from the one for the permeate side, including all the permeate side information in its main equation. In particular, the equation for the retentate side can be written as

$$\nabla|\nabla p|^{(f_2-1)/(2-f_2)}\nabla p = -\left(\frac{f_1\rho^{1-f_2}\mu^{f_2}}{D^{1\ +\ f_2}}\right)^{1+(f_2-1)/(2-f_2)}\frac{k_w}{\delta L_{rz}}\left(p - \sum_{i=0}^{\infty}\sum_{j=1}^{\infty}\frac{(1 + e^{-2\beta_{ij}L_{pz}})}{\beta_{ij} - \beta_{ij}e^{-2\beta_{ij}L_{pz}} + \frac{k_w}{ik_2\delta}(1 + e^{-2\beta_{ij}L_{pz}})}\frac{4}{L_x L_y}\int_0^{L_x}\int_0^{L_y} p(x,y)\cos\left(\frac{i\pi}{L_x}x\right)\sin\left(\frac{j\pi}{2L_y}y\right)\mathrm{d}x\,\mathrm{d}y\cos\left(\frac{i\pi}{L_x}x\right)\sin\left(\frac{j\pi}{2L_y}y\right)\right) \tag{26}$$

This equation is a partial integro-differential equation having as only unknown parameter the pressure field $p(x,y)$. In this way the initial two-domain problem is reduced to a single-domain one.

Knowledge of the three-dimensional permeate pressure field is of rather small practical value because, as it can be deduced from the form of the analytical solution, the variation of the pressure in the Z direction is insignificant due mainly to the small aspect ratios of the gap (L_{pz}) over its two other dimensions. This small variation of the pressure allows introducing a new two-dimensional pressure field $P(x,y)$ corresponding to the local average in the Z direction. Unlike the approach used for the retentate side, this is a formal procedure, as outlined in Appendix C. The governing eq 3 is integrated with respect to Z, and recalling the Z uniformity of the pressure and the boundary conditions, the following equation governing the two-dimensional field $P(x,y)$ is obtained

$$\frac{\partial^2 P}{\partial x^2} + \frac{\partial^2 P}{\partial y^2} = \frac{k_w}{k_1 \delta L_{pz}}(P-p) \tag{27}$$

The first-order correction to the uniform pressure in the Z direction consists of a linear w velocity profile in the Z direction and a quadratic Z dependence of the pressure field.

3. Problem Solution

3.1. Nondimensionalization. It was shown that the two-dimensional pressure field in the membrane element can be obtained from the solution of the coupled partial differential eqs 15 and 27 subject to the boundary conditions (eqs 4a, 4b, 4c, 6c, 6d, and 6e. The proper nondimensionalization of these equations is important for the study of their solution structure. In what follows all the length variables are normalized with the element/membrane width L_y and all the pressures with the operating pressure p_{in}. The normalized variables are subsequently denoted by the subscript "d". The pressure gradient in the permeability term is divided by a reference pressure gradient in order to obtain a value of unity for the reference case of no flux through the membrane. Then, the dimensionless equations take the form (where $p_{od} = p_{out}/p_{in}$)

$$\frac{\partial}{\partial x_d}\left[\frac{L_{xd}}{1-p_{od}}\left(\left(\frac{\partial p_d}{\partial x_d}\right)^2 + \left(\frac{\partial p_d}{\partial y_d}\right)^2\right)^{1/2}\right]^{\alpha}\frac{\partial p_d}{\partial x_d} + \frac{\partial}{\partial y_d}\left[\frac{L_{xd}}{1-p_{od}}\left(\left(\frac{\partial p_d}{\partial x_d}\right)^2 + \left(\frac{\partial p_d}{\partial y_d}\right)^2\right)^{1/2}\right]^{\alpha}\frac{\partial p_d}{\partial y_d} = A(p_d - P_d) \tag{28}$$

$$\frac{\partial^2 P_d}{\partial x_d^2} + \frac{\partial^2 P_d}{\partial y_d^2} = B(P_d - p_d) \tag{29}$$

with the boundary conditions

$$x_d = 0, \frac{\partial P_d}{\partial x_d} = 0,\ p_d = 1 \tag{30a}$$

$$x_d = L_{xd}, \frac{\partial P_d}{\partial x_d} = 0,\ p_d = p_{od} \tag{30b}$$

$$y_d = 0,\ P_d = 0, \frac{\partial p_d}{\partial y_d} = 0 \tag{30c}$$

$$y_d = 1,\ \frac{\partial P_d}{\partial y_d} = 0, \frac{\partial p_d}{\partial y_d} = 0 \tag{30d}$$

The three dimensionless variables appearing in the problem are given as

$$\alpha = \frac{f_2 - 1}{2 - f_2} \tag{31}$$

$$B = \frac{k_w L_y^2}{k_1 \delta L_{pz}} \tag{32}$$

$$A = \left(\frac{f_1 \rho^{1-f_2} \mu^{f_2}}{D^{1+f_2}}\right)^{1/(2-f_2)} \left(\frac{L_x}{p_{in} - p_{out}}\right)^{(f_2-1)/(2-f_2)} \frac{k_w L_y^2}{k_1 \delta L_{rz}} \tag{33}$$

Obviously the mathematical problem is determined by four dimensionless parameters, i.e., A, B, p_{od}, and α. Parameter α can take values from 0 to -1 and expresses the degree of nonlinearity of the flow resistance law ($\alpha = 0$ for the linear case, i.e., Darcy's law). Parameter B expresses the ratio of the membrane permeability to the permeate side permeability and determines the pressure drop at the permeate side (i.e., the larger the B value the greater the pressure drop at the permeate side). Finally, parameter A represents the ratio of the membrane permeability to the retentate side permeability. In the present setup of the problem, i.e., imposed retentate outflow pressure p_{out} instead of flow rate (which is a common operating mode in practice), A is related to the fraction of the inlet flow permeating through the membrane (fluid recovery).

According to the suggestion of Aris,[26] having a mathematical model of a system, it is important to explore and understand the structure of its solution before providing specific results for specific realistic operating conditions. Therefore, the first step here is the study of simplified cases which allows isolation of the key parameters and study of their influence using analytical or approximating solution techniques.

3.2. Simplified Cases. 3.2.1. No Pressure Drop at the Permeate Side ($B = 0$). In this case the permeate side pressure field is zero everywhere. The retentate side problem has no y dependence, and it is therefore transformed to the following one-dimensional boundary value problem

$$\frac{\partial}{\partial x_d}\left[\frac{L_{xd}}{1-p_{od}}\left|\frac{\partial p_d}{\partial x_d}\right|\right]^{\alpha}\frac{\partial p_d}{\partial x_d} = A p_d \text{ with } BC\ p_d(0) = 1,\ p_d(L_{xd}) = p_{od} \tag{34}$$

From the solution of this problem one can determine the pressure drop profile but also a more significant quantity, *fluid recovery* F, i.e., the fraction of the inlet flow permeating the membrane, which can be computed as

$$F = 1 - \left|\left(\frac{\partial p_d}{\partial x_d}\right)_{x_d = L_{xd}}\right|^{\alpha+1}\left|\left(\frac{\partial p_d}{\partial x_d}\right)_{x_d = 0}\right|^{-\alpha-1} \tag{35}$$

For the particular case $\alpha = 0$, the problem is linear and the following analytical solution is obtained

$$p_d = c_1 e^{-\sqrt{A}x_d} + c_2 e^{\sqrt{A}x_d} \tag{36}$$

$$F = 1 - \frac{c_2 e^{\sqrt{A}L_{xd}} - c_1 e^{-\sqrt{A}L_{xd}}}{c_2 - c_1} \tag{37}$$

where

$$c_1 = \frac{e^{\sqrt{A}L_{xd}} - p_{od}}{e^{\sqrt{A}L_{xd}} - e^{-\sqrt{A}L_{xd}}} \tag{38a}$$

$$c_2 = \frac{p_{od} - e^{-\sqrt{A}L_{xd}}}{e^{\sqrt{A}L_{xd}} - e^{\sqrt{A}L_{xd}}} \quad (38b)$$

An analytical solution of the same type has been derived by Karode[27] for the geometrically different but mathematically similar problem of flow through a porous channel or pipe. The fraction of the feed flow rate exiting as retentate ($1 - F$) versus the parameter $A^{0.5}L_{xd}$, for several values of the dimensionless outlet pressure p_{od}, is shown in Figure 3. It is noted that in a typical operation of membrane modules, where the pressure drop is up to 5% (i.e., $p_{od} > 0.95$) the fluid recovery fraction is also 5% (i.e., $F < 0.05$). The pressure profile is linear for $A = 0$. With increasing A, the pressure profile exhibits some curvature. Even when this curvature is small, the slopes at the edges and correspondingly F are strongly dependent on the value of A. With increasing A, the model predicts that the recovery fraction increases up to a value of A for which no outlet flow exists. It is noted that the parameters p_o and A are not independent since the outlet pressure is included also in A. An important outcome of the above analysis is that the parameter A takes very small values, on the order of 10^{-3}, for operation of membrane elements of practical interest.

The next step is the study of the influence of the exponent α on the pressure profile. In the usual case of nonzero exponent α, eq 34 and related boundary conditions constitute a nonlinear two-point boundary value problem, which is solved numerically using a finite difference technique. The pressure profile for the linear flow resistance ($\alpha = 0$) is compared with that for a typical value of the exponent in practice[10] ($\alpha = -0.4$) for two values of the parameter $A^{0.5}L_{xd}$ in Figure 4. The negative exponent implies an increase of resistance to flow and a greater pressure drop increase, compared to the $\alpha = 0$ case, as shown in Figure 4. It is worth noting that although the fluid recovery fraction is 0.3 (outside of the practical operating regime) for the case $A^{0.5}L_x = 0.2$ the effect of the exponent α on the pressure profile is very small. Also, the effect of α on F is insignificant. In addition, it is interesting that even for this large fraction of water permeating the membrane the pressure variation is still close to a linear one. Only for cases like the one with $A^{0.5}L_{xd} = 0.4$ (87% of the flow through the membrane, of no practical interest) α significantly influences the pressure profile and F. The fact that under practical conditions α does not influence the pressure

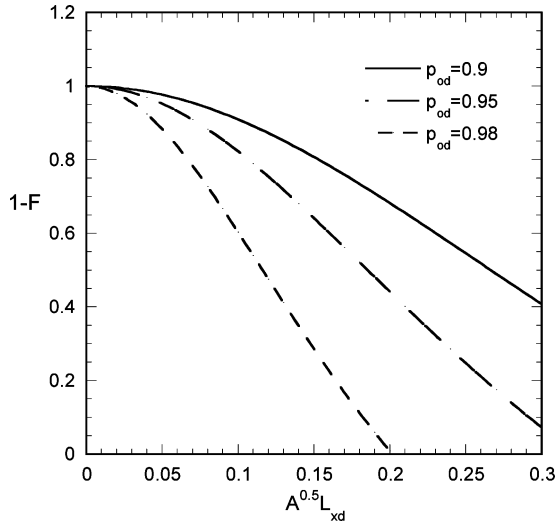

Figure 3. Fraction of fluid exiting at the retentate side vs parameter A for several values of pressure p_{od} ($B = 0$, $\alpha = 0$).

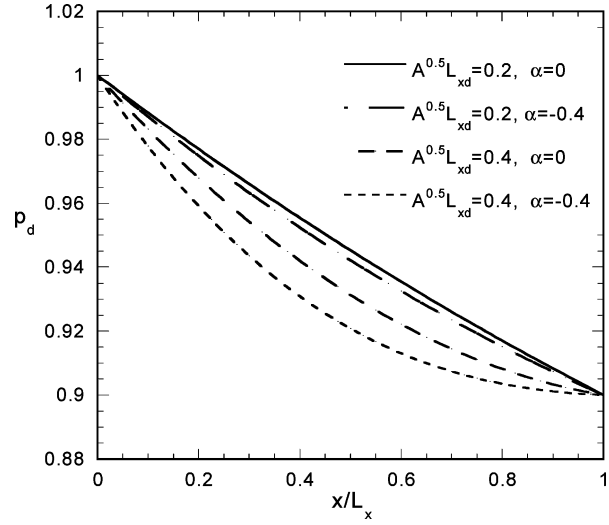

Figure 4. Retentate side pressure profile along the flow for two values of parameter A and two values of exponent α ($\beta = 0$).

profile and the fluid recovery fraction F does not mean that it can be totally ignored since it actually determines the inlet flow rate.

3.2.2. Negligible Flow Fraction through the Wall ($A = 0$). This condition implies that an insignificant amount of the feed flow permeates the membrane and leads directly to the following expression for the pressure: $p_d = 1 - \gamma x_d$, where $\gamma = (1 - p_{od})/L_{xd}$. According to the discussion of results presented in Figure 3, this pressure profile is a good approximation not only for $A = 0$ but for all values of A encountered in practice. The equation for the permeate pressure field takes the form

$$\frac{\partial^2 P_d}{\partial x_d^2} + \frac{\partial^2 P_d}{\partial y_d^2} = B(P_d - 1 + \gamma x_d) \quad (39)$$

This equation does not have an analytical solution, but it can be solved approximately as follows: The variation of the pressure field in the y direction is very strong, and it is determined by the essential boundary condition $P = 0$ at $y = 0$. On the other hand, the variation in the x direction is weak and emerges from the source term ($1 - \gamma x_d$) in eq 39. This term actually undergoes a smoothing by the x-second derivative term. For large values of B or large aspect ratio (L_{xd}) the smoothing term can be ignored rendering the problem one-dimensional with x_d as parameter. This problem can be solved analytically, leading to

$$P_d = \frac{\gamma x_d - 1}{1 + e^{-2\sqrt{B}}} e^{-2\sqrt{B}y_d} + \frac{\gamma x_d - 1}{1 + e^{-2\sqrt{B}}} e^{\sqrt{B}(y_d - 2)} + 1 - \gamma x_d \quad (40)$$

Equation 39 was also solved using a finite element technique. The analytical and numerical y-direction profiles of permeate pressure are shown for three positions along the flow in Figure 5 for the case $B = 3$, $L_{xd} = 10$. The profiles from the two types of solution are very close to each other; only those for $(x/L_x) = 1$ differ somewhat. The evolution of the pressure at $y_d = 1$ along the flow is shown in Figure 6 for several values of B. Obviously the larger the B value, the greater the pressure drop increase at the permeate side. The analytical solution is an excellent approximation of the numerical one under the conditions examined here, and it reveals the structure of the pressure field in the permeate side for a large aspect ratio membrane module.

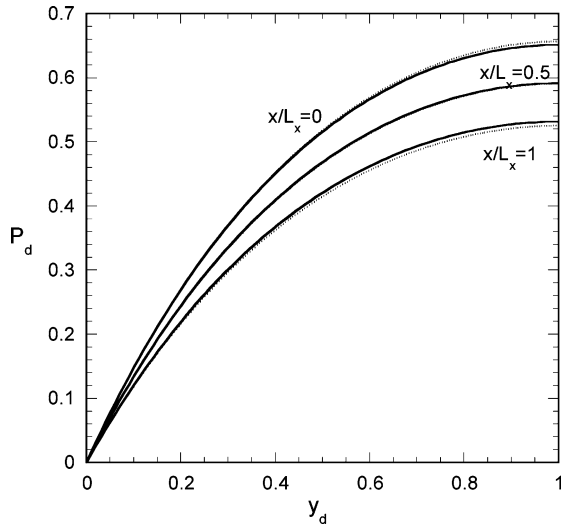

Figure 5. Permeate side pressure profile at three locations along the flow. Comparison between numerical and approximate analytical results ($A = 0$, $\beta = 3$). Solid lines depict the numerical solution and dotted lines the analytical results.

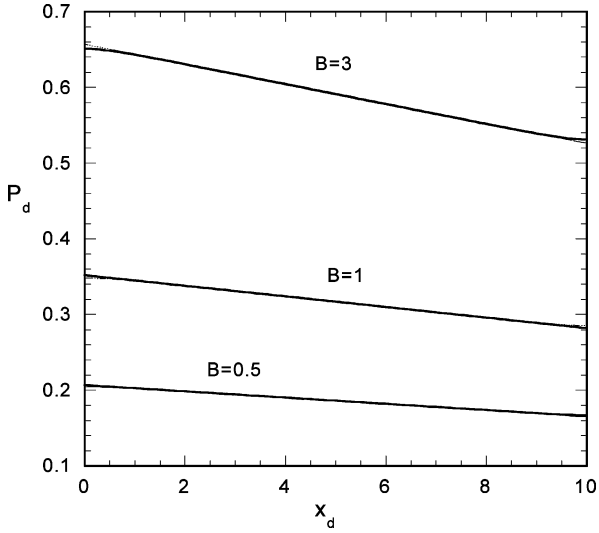

Figure 6. Permeate side pressure variation at $y = L_y$ in the main flow direction for several values of B ($A = 0$).

3.3. On the *y* Dependence of the Retentate Pressure Field. We consider the most general form of the retentate side equation where the effective membrane permeability is nonuniform (e.g., due to fouling). The corresponding equation has the following form (assuming for this analysis that $\alpha = 0$, since it was shown above that α does not significantly influence the pressure field)

$$\frac{\partial^2 p_d}{\partial x_d^2} + \frac{\partial^2 p_d}{\partial y_d^2} = A(x_d,y_d)(p_d - P_d(x_d,y_d)) \qquad (41)$$

The y dependence of the field is imposed through the y dependence of A and P_d. However, as it was shown above, A has to be a very small number (on the order of 10^{-3}) under practical conditions. This means that the diffusion-like term in eq 41 is much stronger than the source term and tends to spread instantaneously any y nonuniformity imposed by the source. The implication of the above observation is that the pressure field in the retentate side is practically one-dimensional, and it can be determined from the following equation, obtained by integrating in the y direction and using the boundary condition and y uniformity of p_d

$$\frac{\partial^2 p_d}{\partial x_d^2} = \int_0^1 A(x_d,y_d)(p_d - P_d(x_d,y_d))dy_d \qquad (42)$$

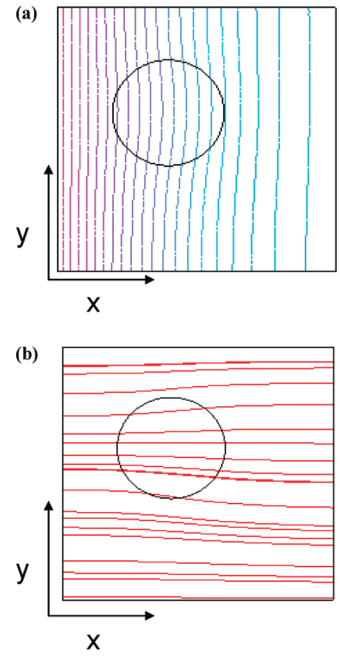

Figure 7. (a) Isobaric lines and (b) streamlines at the retentate side for the case of a disk-type membrane region of zero permeability ($B = 0, \alpha = 0$).

In order to test the validity of the above arguments an extreme retentate side problem ($B = 0$, $\alpha = 0$, $p_{od} = 0.9$) is set up. The aspect ratio is one ($L_{xd} = 1$), the value of A is such that $F = 1$ (i.e., all the flow goes through the membrane), and there is a patch on the membrane with zero permeability. This problem is solved using finite elements. The isobaric lines are plotted in Figure 7, showing that there is a small deviation from the uniformity in the y direction, i.e., smaller than 5% of the pressure drop. Under practical conditions ($F < 0.1$) and smaller permeability differences, the pressure nonuniformity is at least one order of magnitude smaller than the one shown here and it may be safely ignored. The flow streamlines are shown in Figure 7b; apparently there is a slight transverse motion of the fluid to compensate for the wall flux nonuniformity, but under practical conditions the direction of the flow can be considered uniform. The implications of the above observations are 2-fold. First, the two-dimensional partial differential equation for the retentate pressure field can be conveniently replaced by the one-dimensional eq 42. Second, the direction of the flow at the retentate side tends to remain unchanged; thus, there is no reason for computing the resistance law for angle θ different than 90°.

3.4. Membrane Element Operation under Practical Conditions. The above findings are integrated for the development of a computational code for determining the pressure fields in a membrane element, where eq 41 is used for the retentate side. The code can be used to compute the pressure distribution and the flow velocities in a membrane element operating under realistic conditions. Four types of spacer geometry are considered. Case A: $\beta = 90°$, $H/D = 6$. Case B: $\beta = 90°$, $H/D = 8$. Case C: $\beta = 90°$, $H/D = 12$. Case D: $\beta = 120°$, $H/D = 6$. The corresponding values for f_1 and f_2 are taken from previous work.[10] The dimensions of the elements are 0.8 × 0.8 m and

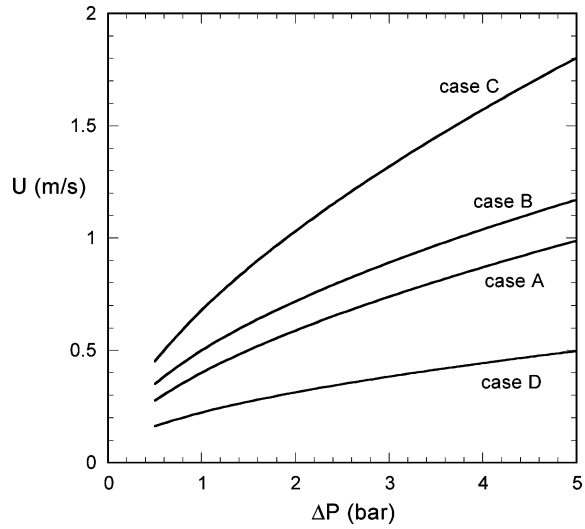

Figure 8. Inlet feed flow velocity U vs pressure drop at the retentate side for several types of spacers ($B = 0$).

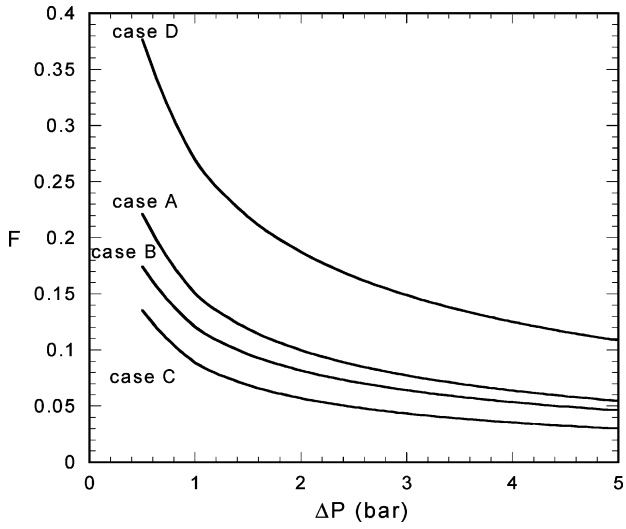

Figure 9. Fluid recovery fraction F vs pressure drop at the retentate side for several types of spacers ($B = 0$).

the operating pressure 20 bar. The rest of the parameters are fixed to values corresponding to typical values of inlet velocity and membrane flux (similar to those shown in a literature example[2]). A sensitivity study is performed with respect to the pressure drop ΔP and the parameter B. The computation of the inlet flow velocity (uniform in the y direction according to the preceding analysis) and of the fluid recovery fraction F is performed as

$$F = 1 - \left| \left(\frac{\partial p_d}{\partial x_d} \right)_{x_d = L_{xd}} \right|^{1/(2-f_2)} \left| \left(\frac{\partial p_d}{\partial x_d} \right)_{x_d = 0} \right|^{-1/(2-f_2)} \tag{43}$$

$$U = \left(\frac{D^{1+f_2}}{f_1 \rho^{1-f_2} \mu^{f_2}} \frac{p_{in}}{L_y} \left| \left(\frac{\partial p_d}{\partial x_d} \right)_{x_d = 0} \right| \right)^{1/(2-f_2)} \tag{44}$$

The feed flow (inlet) velocity U vs the pressure drop at the retentate side is shown in Figure 8 for several types of spacers. As expected, the velocity tends to increase (in a non linear manner) and the pressure to decrease as the induced spacer resistance to flow increases. In Figure 9 the fluid recovery fraction vs pressure drop is presented. The large variation of F with the pressure drop is misleading; in fact, there is just a small

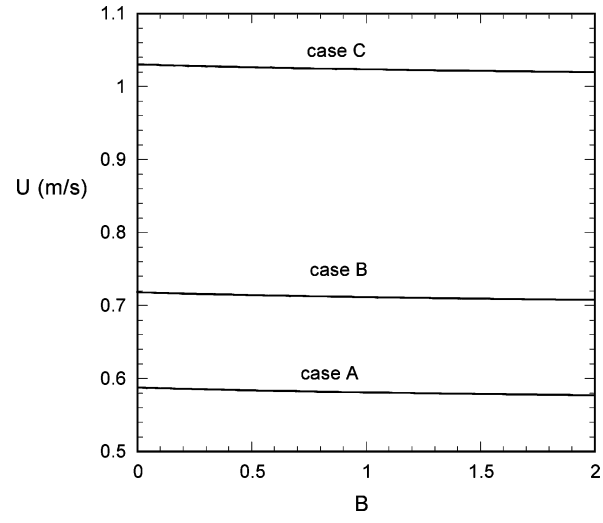

Figure 10. Inlet velocity U vs parameter B for several types of spacers ($\Delta P = 2$ bar).

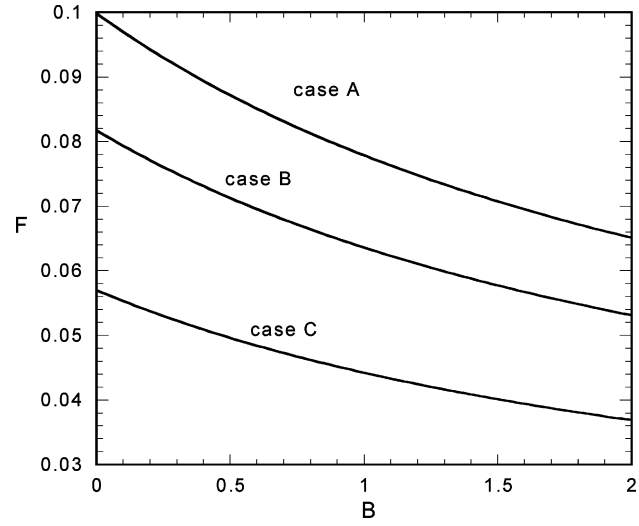

Figure 11. Fluid recovery fraction F vs parameter B for several types of spacers ($\Delta P = 2$ bar).

decrease of the flux through the membrane with the pressure drop due to reduction of the average transmembrane pressure. The flux through the membrane does not depend on the spacer type; the seemingly large variation of F is just due to the compensation in the increase of U to maintain a constant flux. In conclusion, for a given pressure drop the inlet velocity depends on spacer type and the flux through the membrane is fixed.

The influence of the dimensionless parameter B (ratio of membrane to permeate side permeability) is examined next. The following results correspond to a pressure drop of 2 bar. As shown in Figure 10, the influence of B on the velocity U is extremely weak (maximum difference less than 2%). On the contrary, the fraction F (and correspondingly the flux through the membrane if U is constant) depends strongly on B as shown in Figure 11, i.e., as B increases F decreases. The dimensional pressure at $y = L_y$ at the permeate side, along the main flow direction, is shown in Figure 12. The pressure at the permeate side is high for practical purposes, even for $B = 0.5$, implying that in practice values of B smaller than 0.5 must be considered. This longitudinal permeate pressure profile is practically uniform, unlike the case shown in Figure 6, where the pressure profile is linear. The difference here is that the small aspect

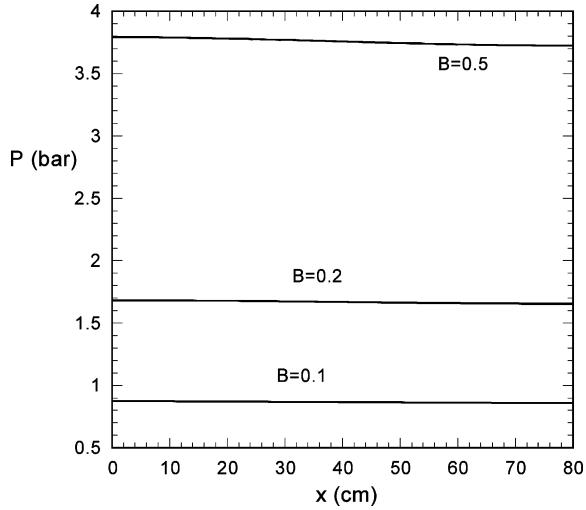

Figure 12. Permeate side pressure variation at $y = L_y$ along the main flow direction for several values of B ($\Delta P = 2$ bar, case A spacers).

ratio of 1 (vs 10 for Figure 6) allows the x-direction second derivative term in eq 41 to eliminate any x-direction nonuniformity of the pressure profile. The effective uniformity of the pressure profile in the x direction suggests the following derivation of an approximate analytical solution for conditions of practical interest in membrane operation.

3.5. Approximate Analytical Solution for Operating Conditions of Practical Interest. First, the permeate side eq 29 is integrated with respect to x, and using the two no flux boundary conditions, the x uniformity of P_d and the y uniformity of p_d, the following equation is obtained

$$\frac{\partial^2 P_d}{\partial y_d^2} = B\left(P_d - \frac{1}{L_{xd}}\int_0^{L_{xd}} p_d(x_d)\mathrm{d}x_d\right) \tag{45}$$

However, as noted above, the linear retentate side pressure profile can be always used for the computation of the transmembrane pressure for practical membrane operations. Thus, substitution in eq 45, performing the right-hand side integration, and then solving the differential equation using the corresponding boundary conditions (eqs 30c and 30d for P_d) leads to

$$P_d = \frac{\gamma L_{xd}/2 - 1}{1 + e^{-2\sqrt{B}}} e^{-\sqrt{B} y_d} + \frac{\gamma L_{xd}/2 - 1}{1 + e^{-2\sqrt{B}}} e^{\sqrt{B}(y_d - 2)} + 1 - \gamma L_{xd}/2 \tag{46}$$

In addition, it was shown that under practical conditions the exponent α has a very small influence on the pressure profile $p_d(x)$. Thus, it is assumed that $\alpha = 0$ and the governing equation for p_d is eq 42. Substitution of the expression for P_d and integration leads to

$$\frac{\partial^2 p_d}{\partial x_d^2} = A\left[p_d - (1 - \gamma L_{xd}/2)\left(1 + \frac{e^{-2\sqrt{B}} - 1}{\sqrt{B}(e^{-2\sqrt{B}} + 1)}\right)\right] \tag{47}$$

Finally, by integrating the above equation, using the corresponding boundary conditions ($p_d = 1$ at $x_d = 0$ and $p_d = p_{od}$ at $x_d = L_{xd}$), the profile of p can be determined as

$$p_d = \frac{(1-Q)e^{\sqrt{A}L_{xd}} - (p_{od} - Q)}{e^{\sqrt{A}L_{xd}} - e^{-\sqrt{A}L_{xd}}} e^{-\sqrt{A}x_d} + \frac{(p_{od} - Q) - (1-Q)e^{-\sqrt{A}L_{xd}}}{e^{\sqrt{A}L_{xd}} - e^{-\sqrt{A}L_{xd}}} e^{\sqrt{A}x_d} + Q \tag{48}$$

where

$$Q = (1 - \gamma L_{xd}/2)\left(1 + \frac{e^{-2\sqrt{B}} - 1}{\sqrt{B}(e^{-2\sqrt{B}} + 1)}\right)$$

Upon substitution of the expression for p (eq 48), in eqs 43 and 44 the velocity U and the fluid recovery can be obtained in closed form. This analytical approximation of the problem leads to exactly the same results as the numerical solution for all conditions of practical interest. Even the weak dependence of B on U is predicted. It is recalled here that the analytical solution is valid only for uniform membrane permeability, and it cannot substitute the numerical code. The latter will be used as the basis for complete simulation of the membrane module operation, including such phenomena as concentration polarization and fouling, leading to spatial nonuniformity of the driving force and of permeability for flow through the membrane.

4. Conclusions and Comments

In this work results are reported of an integrated study of the hydrodynamics of spiral-wound elements starting from first principles. A reduced set of equations is derived, which is characterized by high accuracy and rather small computational effort. All the steps in deriving and simplifying the governing equations are presented and discussed in fair detail. Several analytical approximating solutions for subproblems are obtained, offering guidance in this theoretical analysis. On the basis of the form of governing equations, it is shown that the retentate pressure distribution, in a direction transverse to the main flow, is practically uniform even for the case of nonuniform membrane permeability. An analytical solution is derived for a module operating under practical conditions, but a numerical approach is necessary when nonuniform conditions of membrane permeability prevail. The numerical algorithm for the membrane element hydrodynamics developed here can serve as the basis for global simulation, i.e., for simulation of all aspects of the membrane element operation including mass transfer and fouling, thus facilitating membrane process optimization.

The present work deals with the hydrodynamics in the narrow channels of the SWM module in the absence of a solute, and its extension to include solute separation is required. There are two general approaches in the literature to account for the influence of solute on the hydrodynamics of membrane separators. The first comprises a fully coupled method where the fluid viscosity, density, and solute diffusivity are functions of the local solute concentration.[28] According to the second approach the solute concentration enters in the flow field modeling only through the flux−pressure relation either as effective osmotic pressure (for dissolved substances) or as permeability reduction (for colloidal/particulate substances).[29] A discussion on conditions, under which the second (relatively simpler) approach can be used, is available in the literature.[30] The present analysis and models developed can be rather easily extended to cases

where the effect of solute is considered to cause a (quantifiable) change in the water flux−transmembrane pressure relationship.

Appendices

A. On the Resistance Law for the Permeate Side. In some cases the resistance law in the permeate side may be nonlinear. Indeed, in the literature one can find examples where a linear[3] or nonlinear[31] resistance law is employed. Furthermore, it is of importance to note that the nonlinearity at the permeate side should be handled in a different way than that at the retentate side, as described in detail in the main text. First, a power-type resistance law (e.g., ref 31) is not appropriate in general, since the velocity spans a broad range from zero to a maximum value; thus, the resistance law should be the sum of a linear and nonlinear (power law) term. Nevertheless, the nonlinearity even if it exists is much smaller than that of the retentate channel. In addition, the structure of the porous medium is not well defined, so it can be assumed to be isotropic and the experimentally measured specific permeability relation is appropriate for use in the model. Here only the linear case is considered because the focus is on the analytical aspects of the problem. However, a nonlinear resistance law for the permeate side can be easily incorporated into the numerical algorithm presented in this work.

B. On the Generalized Velocity−Pressure Drop Relation for Flow with Inertia Effects. As discussed in the main text, there is no formal route linking basic eqs 5a, 5b, 5c, and 5d to a generalized form of eq 9, which is employed in the simulations for capturing the essential features of the flow field. Certainly, one cannot claim that the approach used here (explained in some detail below) gives the exact result corresponding to the exact geometry; for instance, concerns regarding the assumed flow periodicity (arising from the inherent unsteadiness of the flow field) are justified, as discussed in the main text. Nevertheless, this approach may be the only possible way if one wishes to obtain the desirable macroscopic scale results by solving the simpler "unit cell" part of the problem; in fact, the latter has already been done to a significant extent.[10,12] Alternatively, one has to solve for the exact geometry of the *entire* flow field, which is more accurate but computationally intractable at present.

It is first recalled that assuming periodicity, Adler has formally shown (pages 175−181 of his book[23]) that the macroscopic velocity U is related to the macroscopic pressure gradient G through a general nonlinear relation, where here the algebraic expansion of his vectorial relation is given

$$U_x = F_1(G_x,G_y;\mu,\rho)$$

$$U_y = F_2(G_x,G_y;\mu,\rho)$$

The dependence on μ and ρ stems from the dependence of the unit cell flow on Reynolds number. The functions F_1, F_2 depend only on unit cell geometry. Further, our proposed generalization of eq 9 for nonlinear flow can be written as

$$U_x = (1/\mu)[K_{11}(U,\theta)\mathrm{i}G_\mathrm{x} + K_{12}(U,\theta)G_y]$$

$$U_y = (1/\mu)[K_{22}(U,\theta)G_y + K_{21}(U,\theta)G_x]$$

In this expression the function K_{ij} depends on μ, ρ (through unit cell Reynolds number), and geometry. The pair of variables U and θ is equivalent to the pair U_x,U_y. It is noted that there is no restriction or loss of generality in going from the above nonlinear functions F_1, F_2 to expression 9 by using a generalized permeability tensor. However, it is considered to be more appropriate to express the general nonlinear interdependence between the macroscopic velocity and pressure gradient, as done in eq 9. Indeed, the specific advantages of the particular form of the relation proposed here is that it tends to the Darcy law in the limit of zero Reynolds number and that it enables exploiting the symmetries and isotropy of the flow field.

C. Directional Averaging of Partial Differential Equations. This technique can be used when the variation of a dependent variable is very small along one direction, and it is applied four times throughout the present work, i.e., along the z direction in permeate and retentate channels, along the y direction in the retentate channel, and along the x direction in the permeate channel. Application of the technique for the Z direction in the permeate channel is explained here. First, one defines

$$P(x,y) = \frac{1}{L_\mathrm{pz}}\int_0^{L_\mathrm{pz}} P(x,y,Z)\mathrm{d}Z$$

Then, taking the integral with respect to Z (from 0 to L_{pz}) of eq 3 and dividing by L_{pz} results in

$$\frac{\partial^2 P}{\partial x^2} + \frac{\partial^2 P}{\partial y^2} + \frac{k_2}{k_1 L_\mathrm{pz}}\left(\frac{\partial P}{\partial Z}\right)_{z\,=\,L_\mathrm{pz}} - \frac{k_2}{k_1 L_\mathrm{pz}}\left(\frac{\partial P}{\partial Z}\right)_{z=0} = 0$$

Substituting the boundary conditions in eqs 4d and 8band the relation 7 leads to

$$\frac{\partial^2 P}{\partial x^2} + \frac{\partial^2 P}{\partial y^2} = \frac{k_\mathrm{w}}{k_1 \delta L_\mathrm{pz}}(P(x,y,0) - p)$$

Knowing that the variation of P in the Z direction is very small, it is assumed that $P(x,y,0) = P(x,y)$, which closes the problem.

Literature Cited

(1) *Membrane Filtration in Water Treatment Principles and Design*; Wiley: New York, 2005; Chapter 12.

(2) Schwinge, J.; Neal, P. R.; Wiley, D. E.; Fletcher, D. F.; Fane, A. G. Spiral wound modules and spacers. Review and analysis. *J. Membr. Sci.* **2004**, *242*, 129–153.

(3) Evangelista, F. Optimal design and performance of spiral wound modules. I. Numerical method. *Chem. Eng. Commun.* **1988**, *72*, 69–81.

(4) Evangelista, F. Optimal design and performance of spiral wound modules. II. Analytical method. *Chem. Eng. Commun.* **1988**, *72*, 81–94.

(5) Evangelista, F. An improved analytical method for the design of spiral wounds modules. *Chem. Eng. J.* **1988**, *38*, 33–40.

(6) Wardeh, S.; Morvan, H. P. CFD simulations of flow and concentration polarization in spacer filler channels for application to water desalination. *J. Chem. Eng. Res. Des.* **2008**, *86*, 1107–1116.

(7) Koutsou, C. P.; Yiantsios, S. G.; Karabelas, A. J. Numerical simulation of the flow in a plane channel containing a periodic array of cylindrical turbulence promoters. *J. Membr. Sci.* **2004**, *231*, 81–90.

(8) Geraldes, V.; Semiao, V.; de Pinho, M. N. The effect of the ladder-type spacers configuration in NF spiral-wound modules on the concentration boundary layers disruption. *Desalination* **2002**, *146*, 187–194.

(9) Geraldes, V.; Semiao, V.; de Pinho, M. N. Flow management in nanofiltration spiral wound modules with ladder type spacers. *J. Membr. Sci.* **2002**, *203*, 87–102.

(10) Koutsou, C. P.; Yiantsios, S. G.; Karabelas, A. J. Direct numerical simulation of flow in spacer-filled channels: Effect of spacer geometrical characteristics. *J. Membr. Sci.* **2007**, *291*, 53–69.

(11) Koutsou, C. P.; Yiantsios, S. G.; Karabelas, A. J. Membrane module performance optimization using CFD simulation of flow through narrow channels with spacers. *Proceedings of the IDA World Congress on Desalination and Water Reuse*; Maspalomas, Gran Canaria, Spain, Oct 21−26, 2007; paper MP07-176.

(12) Koutsou, C. P.; Yiantsios, S. G.; Karabelas, A. J. A numerical and experimental study of mass transfer in spacer-filled channels: Effects of spacer geometrical characteristics and Schmidt number. *J. Membr. Sci.* **2009**, *326*, 234–251.

(13) Ranade, V. V.; Kumar, A. Comparison of flow structures in spacer filled flat and annular channels. *Desalination* **2006**, *191*, 236–244.

(14) Rautenbach, R.; Dahm, W. Design and development of spiral wound and hollow fibre RO-modules. *Desalination* **1987**, *65*, 259–275.

(15) Marinas, B. J.; Urama, R. I. Modeling concentration polarization in reverse osmosis spiral wound elements. *J. Environ. Eng.* **1996**, *122*, 292–298.

(16) Boudinar, M. B.; Hanbury, W. T.; Avlonitis, S. Numerical simulation and optimization of spiral wound modules. *Desalination* **1992**, *86*, 273–290.

(17) Li, Y.-L.; Tung, K.-L. The effect of curvature of a spacer-filled channel on the fluid flow in spiral-wound membrane modules. *J. Membr. Sci.* **2008**, *319*, 286–297.

(18) Ranade, V. V.; Kumar, A. Fluid dynamics of spacer filled rectangular and curvilinear channels. *J. Membr. Sci.* **2006**, *271*, 1–15.

(19) Ahmad, A. L.; Lau, K. K.; Abu Bakar, M. Z. Impact of different spacer filament geometries on concentration polarization control in narrow membrane channel. *J. Membr. Sci.* **2005**, *262*, 138–152.

(20) Da Costa, A. R.; Fane, A. G.; Fell, C. J. D.; Franken, A. C. M. Optimal channel spacer design for ultrafiltration. *J. Membr. Sci.* **1991**, *62*, 275–291.

(21) Kevorkian, J.; Cole J. D. *Multiple scale and singular perturbation methods*; Springer: New York, 1996.

(22) Brenner, H.; Edwards, D. A. *Macrotransport processes*; Butterworth-Heinemann: London, 1993.

(23) Adler, P. M. *Porous Media, Geometry and Transports*; Butterworth-Heinemann: London, 1992.

(24) Bird, R. B.; Stewart, W. E.; Lightfoot, E. N. *Transport phenomena*; Wiley: New York, 1965.

(25) Kaviany, M. *Principles of heat transfer in porous media*; Springer-Verlag: New York, 1991.

(26) Aris, R. *Mathematical modeling techniques*; Dover: New York, 1994.

(27) Karode, S. K. Laminar flow in channels with porous walls, revisited. *J. Membr. Sci.* **2001**, *191*, 237–241.

(28) Bessiere, Y.; Fletcher, D. F.; Bacchin, P. Numerical simulation of colloid dead-end filtration: Effect of membrane characteristics and operating conditions on matter accumulation. *J. Membr. Sci.* **2008**, *313*, 52–59.

(29) Pak, A.; Mohammadi, T.; Hosseinalipour, S. M.; Allahdini, V. CFD modeling of porous membranes. *Desalination* **2008**, *222*, 482–488.

(30) Kim, A. S. Permeate flux injection due to concentration polarization in crossflow membrane filtration: A novel analytic approach. *Eur. Phys. J. E* **2007**, *24*, 331–341.

(31) Van der Meer, W. G. J.; Van Dijk, J. C. Theoretical optimization of spiral wound and capillary nanofiltration modules. *Desalination* **1997**, *113*, 129–146.

Received for review July 13, 2009
Revised manuscript received September 29, 2009
Accepted September 30, 2009

IE901129J